Supporting Information for: Force Field for Mg^{2+}, Mn^{2+}, Zn^{2+} and Cd^{2+} Ions That Have Balanced Interactions with Nucleic Acids

Maria T. Panteva, George M. Giambaşu, and Darrin M. York*

Center for Integrative Proteomics Research, BioMaPS Institute and Department of Chemistry & Chemical Biology, Rutgers University, 174 Frelinghuysen Road, Piscataway, NJ 08854-8076, USA

E-mail: Darrin.York@rutgers.edu

*To whom correspondence should be addressed

Mg^{2+} ion parameters - nucleic acid site binding free energies

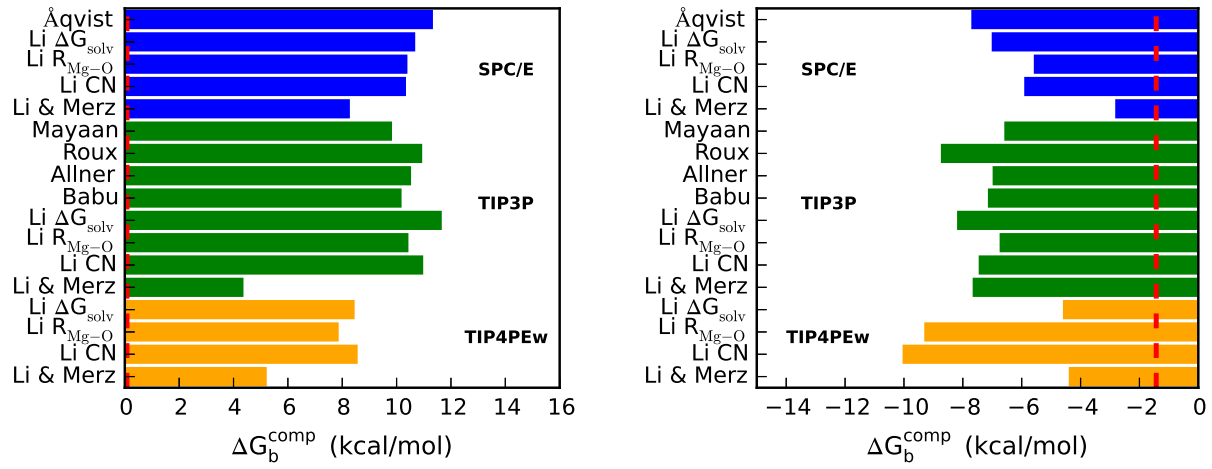

(a) Mg^{2+} bound to adenosine.

(b) Mg^{2+} bound to dimethyl phosphate.

Figure S1: Summary of computed site specific binding free energies between 17 pairwise Mg^{2+} models and a) the N7 atom of adenosine and b) the non-bridging oxygen of dimethyl phosphate (DMP), grouped by water model and compared with experiment (dashed red line).

Comparison of 12-6-4 and m12-6-4 divalent ion parameters interacting with model systems

Table S1: Comparison of 12-6-4 and m12-6-4 polarizabilities for Mg^{2+}, Mn^{2+}, Zn^{2+} and Cd^{2+} interacting with the N7 of adenosine, guanosine ($\alpha_{A:N7}$, $\alpha_{G:N7}$) or the non-bridging oxygen of dimethyl phosphate ($\alpha_{DMP:OP}$). Polarizabilities are in units of Å^3.

	12-6-4			m12-6-4		
Ion	$\alpha_{DMP:OP}$	$\alpha_{A:N7}$	$\alpha_{G:N7}$	$\alpha_{DMP:OP}$	$\alpha_{A:N7}$	$\alpha_{G:N7}$
Mg^{2+}	0.569	1.090	1.090	0.170	1.910	1.925
Mn^{2+}	0.569	1.090	1.090	0.370	1.770	1.860
Zn^{2+}	0.569	1.090	1.090	0.510	1.480	1.640
Cd^{2+}	0.569	1.090	1.090	0.680	1.580	1.920

Table S2: Comparison of the absolute binding free energies for the 12-6-4 and modified 12-6-4 (m12-6-4) divalent ion models interacting with the specific nucleic acid sites and compared with experiment.[1] Free energies are in kcal/mol.

	Ion	Phosphate	Adenosine	Guanosine
Expt.	Mg^{2+}	-1.43	0.08 ± 0.20	-0.34 ± 0.34
	Mn^{2+}	-1.77	-0.05 ± 0.12	-0.64 ± 0.27
	Zn^{2+}	-1.77	-0.20 ± 0.05	-1.45 ± 0.15
	Cd^{2+}	-1.91	-0.87 ± 0.04	-1.95 ± 0.10
12-6-4	Mg^{2+}	-4.56 ± 0.21	4.89 ± 0.26	4.50 ± 0.23
	Mn^{2+}	-3.19 ± 0.25	3.30 ± 0.28	3.06 ± 0.11
	Zn^{2+}	-2.47 ± 0.15	3.18 ± 0.23	3.34 ± 0.16
	Cd^{2+}	-1.13 ± 0.31	1.60 ± 0.19	2.14 ± 0.32
m12-6-4	Mg^{2+}	-1.39 ± 0.20	0.18 ± 0.30	-0.24 ± 0.24
	Mn^{2+}	-1.71 ± 0.24	0.02 ± 0.28	-0.55 ± 0.14
	Zn^{2+}	-1.75 ± 0.13	-0.21 ± 0.23	-1.42 ± 0.16
	Cd^{2+}	-1.91 ± 0.33	-0.80 ± 0.19	-2.01 ± 0.26

Table S3: Comparison of data extracted from free energy profiles for ion dissociation from nucleic acid sites for the 12-6-4 and m12-6-4 ions models: $R^{\dagger}$ - transition state distance (Å), R_{min1} - equilibrium direct contact distance (Å), A_1 - pre-exponential factor (fs^{-1}) for ion dissociation, $\Delta G_1^{\dagger}$ - activation free energy for ion dissociation (kcal/mol), log(k_1) - log of dissociation rate. All properties denoted with "-1" are for the association process of each ion with the nucleic acid sites. Standard deviations come from four consecutive 2 ns segments of data. k_1/k_{-1} is the ion dissociation/association ratio for each ion - nucleic acid interaction.

		Ion	$R^{\dagger}$	R_{min1}	A_1	$\Delta G_1^{\dagger}$	log(k_1)	k_1	R_{min-1}	A_{-1}	$\Delta G_{-1}^{\dagger}$	log(k_{-1})	k_{-1}	k_1/k_{-1}
12-6-4	Dimethyl phosphate	Mg^{2+}	2.65 ± 0.01	2.00 ± 0.00	0.022	13.5 ± 0.2	3.4 ± 0.3	2.8×10^3	4.17 ± 0.04	0.005	7.5 ± 0.2	7.2 ± 0.3	1.5×10^7	0.0002
		Mn^{2+}	2.73 ± 0.03	2.07 ± 0.00	0.018	8.9 ± 0.2	6.7 ± 0.3	$5.2 \times 1\,0^6$	4.30 ± 0.07	0.004	5.7 ± 0.4	8.4 ± 0.5	2.6×10^8	0.0200
		Zn^{2+}	2.64 ± 0.02	2.01 ± 0.00	0.018	11.7 ± 0.2	4.7 ± 0.3	4.8×10^4	4.21 ± 0.03	0.004	7.5 ± 0.1	7.1 ± 0.1	1.4×10^7	0.0034
		Cd^{2+}	2.95 ± 0.01	2.17 ± 0.00	0.012	6.5 ± 0.0	8.3 ± 0.0	2.1×10^8	4.41 ± 0.01	0.005	3.9 ± 0.2	9.8 ± 0.3	6.4×10^9	0.0328
	Adenosine	Mg^{2+}	2.62 ± 0.01	2.17 ± 0.00	0.015	5.8 ± 0.1	8.9 ± 0.1	8.2×10^8	4.34 ± 0.04	0.004	8.6 ± 0.1	6.3 ± 0.1	1.8×10^6	455.6
		Mn^{2+}	2.80 ± 0.04	2.27 ± 0.01	0.009	1.5 ± 0.1	11.8 ± 0.1	6.9×10^{11}	4.52 ± 0.03	0.004	3.6 ± 0.3	9.9 ± 0.4	8.4×10^9	82.1
		Zn^{2+}	2.57 ± 0.02	2.15 ± 0.00	0.014	5.3 ± 0.2	9.3 ± 0.3	1.8×10^9	4.29 ± 0.03	0.004	7.4 ± 0.1	7.2 ± 0.1	1.5×10^7	120.0
		Cd^{2+}	3.05 ± 0.01	2.39 ± 0.01	0.008	1.8 ± 0.1	11.6 ± 0.1	3.7×10^{11}	4.60 ± 0.05	0.002	2.6 ± 0.1	10.5 ± 0.1	3.0×10^{10}	12.3
	Guanosine	Mg^{2+}	2.61 ± 0.00	2.18 ± 0.00	0.015	5.2 ± 0.1	9.3 ± 0.1	2.1×10^9	4.25 ± 0.06	0.004	7.9 ± 0.2	6.8 ± 0.3	6.2×10^6	338.7
		Mn^{2+}	2.79 ± 0.02	2.29 ± 0.01	0.008	1.3 ± 0.1	12.0 ± 0.1	9.3×10^{11}	4.47 ± 0.09	0.004	3.1 ± 0.1	10.3 ± 0.1	1.9×10^{10}	48.9
		Zn^{2+}	2.55 ± 0.02	2.16 ± 0.00	0.014	4.8 ± 0.2	9.6 ± 0.4	4.0×10^9	4.19 ± 0.04	0.003	6.9 ± 0.1	7.4 ± 0.1	2.6×10^7	153.8
		Cd^{2+}	2.89 ± 0.03	2.40 ± 0.01	0.006	1.2 ± 0.1	11.9 ± 0.1	7.8×10^{11}	4.56 ± 0.08	0.003	2.3 ± 0.3	10.8 ± 0.4	6.6×10^{10}	11.8
m12-6-4	Dimethyl phosphate	Mg^{2+}	2.59 ± 0.01	2.02 ± 0.00	0.020	12.0 ± 0.2	4.5 ± 0.3	3.4×10^4	4.21 ± 0.04	0.004	8.6 ± 0.1	9.1 ± 0.1	1.7×10^6	0.0200
		Mn^{2+}	2.82 ± 0.02	2.07 ± 0.00	0.017	8.3 ± 0.1	7.1 ± 0.1	$1.4 \times 1\,0^7$	4.39 ± 0.00	0.007	5.1 ± 0.3	9.1 ± 0.4	1.3×10^9	0.0108
		Zn^{2+}	2.65 ± 0.01	2.01 ± 0.00	0.018	11.5 ± 0.1	4.8 ± 0.1	6.8×10^4	4.21 ± 0.03	0.004	8.0 ± 0.2	6.7 ± 0.3	4.7×10^6	0.0145
		Cd^{2+}	2.96 ± 0.02	2.16 ± 0.00	0.013	7.1 ± 0.1	7.9 ± 0.1	8.0×10^7	4.47 ± 0.02	0.005	4.0 ± 0.1	9.8 ± 0.1	6.0×10^9	0.0133
	Adenosine	Mg^{2+}	2.66 ± 0.01	2.12 ± 0.00	0.017	8.5 ± 0.1	7.0 ± 0.1	9.5×10^6	4.24 ± 0.05	0.004	6.6 ± 0.2	7.7 ± 0.3	5.5×10^7	0.1727
		Mn^{2+}	2.96 ± 0.02	2.22 ± 0.00	0.011	3.9 ± 0.1	10.2 ± 0.1	1.7×10^{10}	4.37 ± 0.03	0.004	2.3 ± 0.2	10.9 ± 0.3	8.7×10^{10}	0.1954
		Zn^{2+}	2.68 ± 0.02	2.13 ± 0.00	0.016	7.4 ± 0.2	7.8 ± 0.3	5.8×10^7	4.25 ± 0.04	0.003	6.1 ± 0.1	8.0 ± 0.1	1.1×10^8	0.5273
		Cd^{2+}	3.29 ± 0.01	2.34 ± 0.01	0.010	3.7 ± 0.0	10.2 ± 0.0	1.8×10^{10}	4.46 ± 0.02	0.004	1.7 ± 0.3	11.3 ± 0.4	2.1×10^{11}	0.0857
	Guanosine	Mg^{2+}	2.64 ± 0.01	2.14 ± 0.00	0.016	7.8 ± 0.3	7.5 ± 0.4	3.2×10^7	4.22 ± 0.03	0.004	6.1 ± 0.1	8.1 ± 0.1	1.4×10^8	0.2286
		Mn^{2+}	2.97 ± 0.01	2.22 ± 0.00	0.011	3.8 ± 0.1	10.3 ± 0.1	2.0×10^{10}	4.30 ± 0.07	0.003	1.5 ± 0.1	11.3 ± 0.1	2.1×10^{11}	0.0952
		Zn^{2+}	2.66 ± 0.01	2.13 ± 0.00	0.016	7.6 ± 0.2	7.7 ± 0.3	4.6×10^7	4.15 ± 0.07	0.003	4.9 ± 0.2	8.9 ± 0.3	8.4×10^8	0.0548
		Cd^{2+}	3.46 ± 0.06	2.30 ± 0.00	0.009	3.8 ± 0.1	10.1 ± 0.1	1.4×10^{10}	4.55 ± 0.03	0.003	1.1 ± 0.1	11.6 ± 0.1	4.3×10^{11}	0.0326

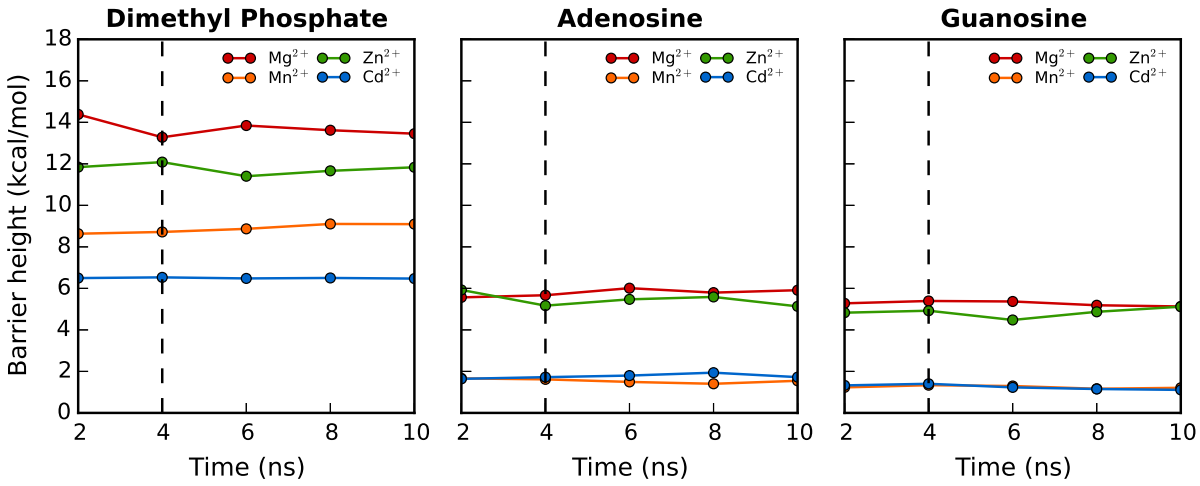

(a) 12-6-4 divalent ion parameters.

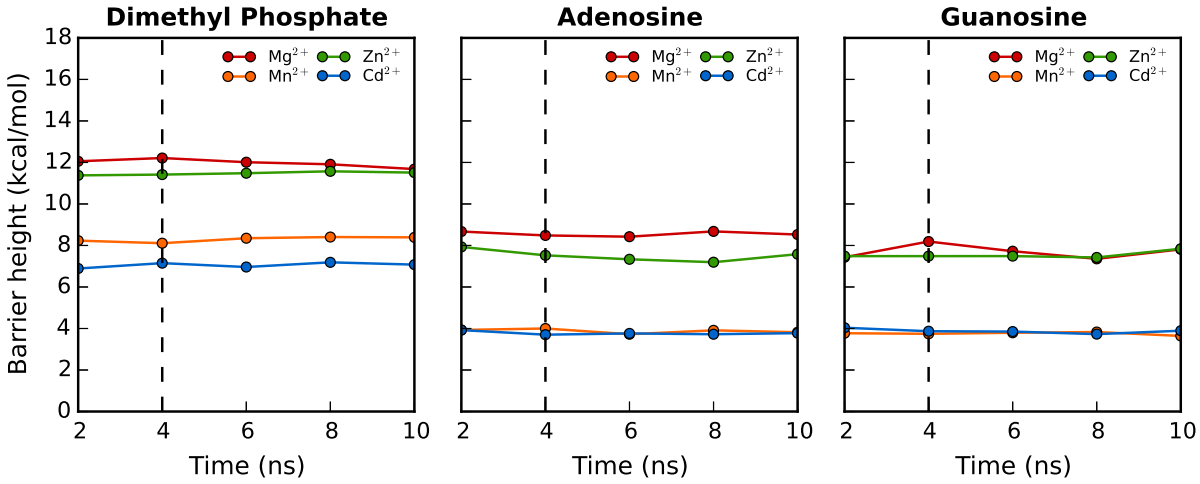

(b) m12-6-4 divalent ion parameters.

Figure S2: Barrier heights for ion dissociation of a) 12-6-4 and b) m12-6-4 Mg^{2+}, Mn^{2+}, Zn^{2+} and Cd^{2+} ion models from specific nucleic acid sites obtained using data gathered from 41 umbrella windows, each 10 ns in length. Each data point on the plot represents the computed barrier height for a 2 ns segment up to that point. The final reported barriers and error estimates were obtained by averaging the barriers from the last 8 ns and computing their respective standard deviations. Left: Dimethyl phosphate, Middle: Adenosine, Right: Guanosine.

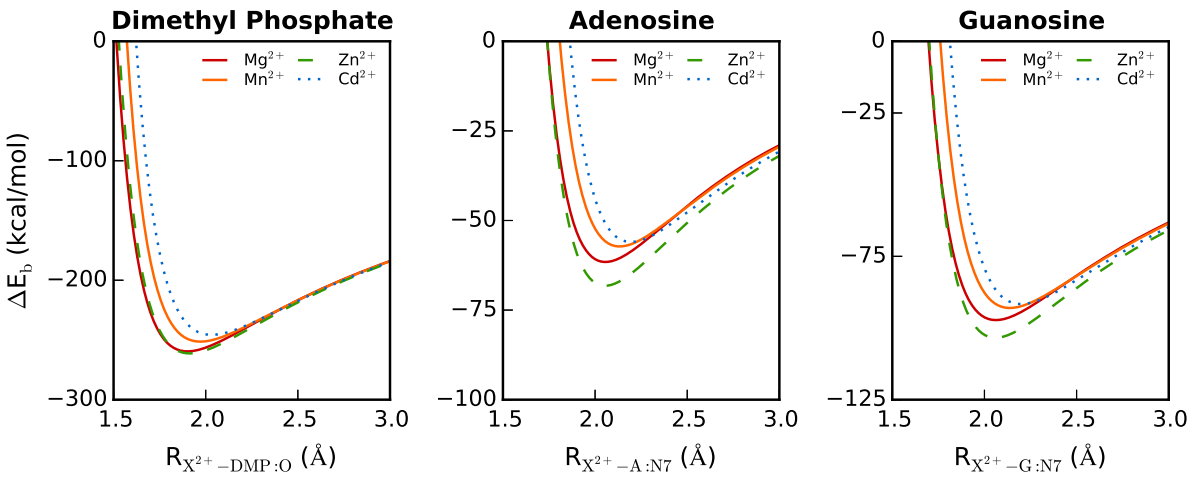

(a) 12-6-4 divalent ion parameters.

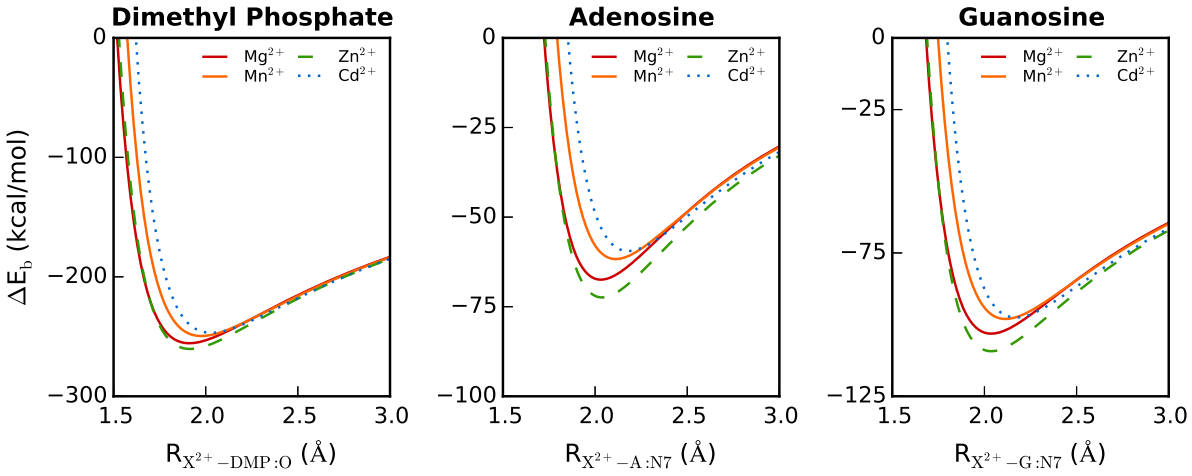

(b) m12-6-4 divalent ion parameters.

Figure S3: Comparison of total binding energy (ΔE_b) for Mg^{2+}, Mn^{2+}, Zn^{2+} or Cd^{2+} and dimethyl phosphate (DMP), adenosine (A) or guanosine (G) in the gas phase versus ion - nucleic acid site separation distance ($R_{X^{2+}\text{-nucleic acid site}}$).

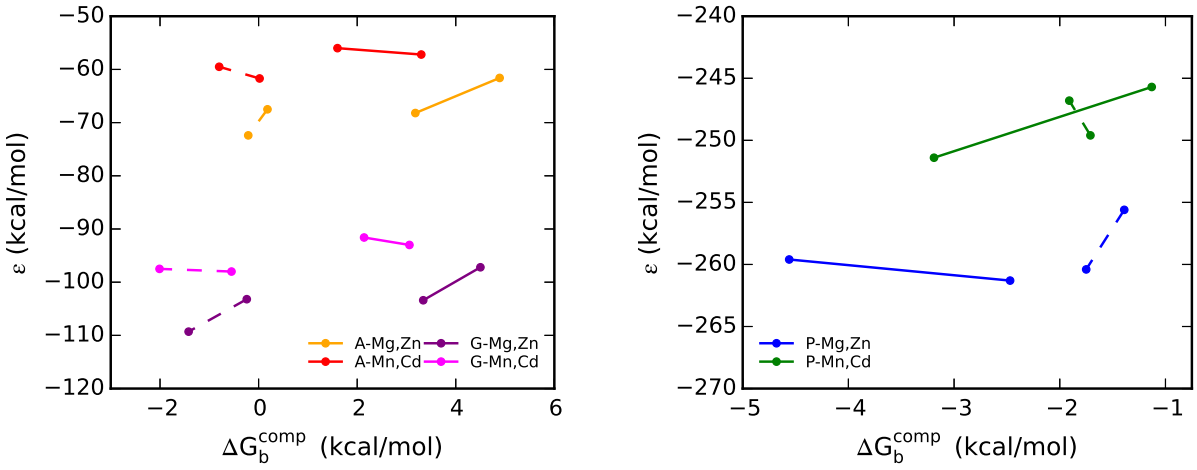

(a) Ion - nucleoside binding.

(b) Ion - dimethyl phosphate binding.

Figure S4: Comparison of total gas phase binding energies (ε) and computed absolute binding free energies (ΔG_b^{comp}) for both 12-6-4 and m12-6-4 ion models binding to a) nucleoside and b) dimethyl phosphate sites. Marker colors distinguish the types of interactions based on not only nucleic acid site but also the identity of the divalent metal ion. The cations are grouped based on model ionic radius, with Mg^{2+} and Zn^{2+} making up one group and Mn^{2+} and Cd^{2+} making up another. m12-6-4 models can be distinguished from 12-6-4 models by the use of dashed lines.

In order to gain further insight into the origin of the differences in ε for the ions binding to guanosine vesus adenosine, we have also performed relaxed gas-phase energy scans for all the metal ion - nucleoside interactions. Below we compare the rigid gas-phase energy scan curves (which are discussed in the main text) with the relaxed gas-phase energy scans.

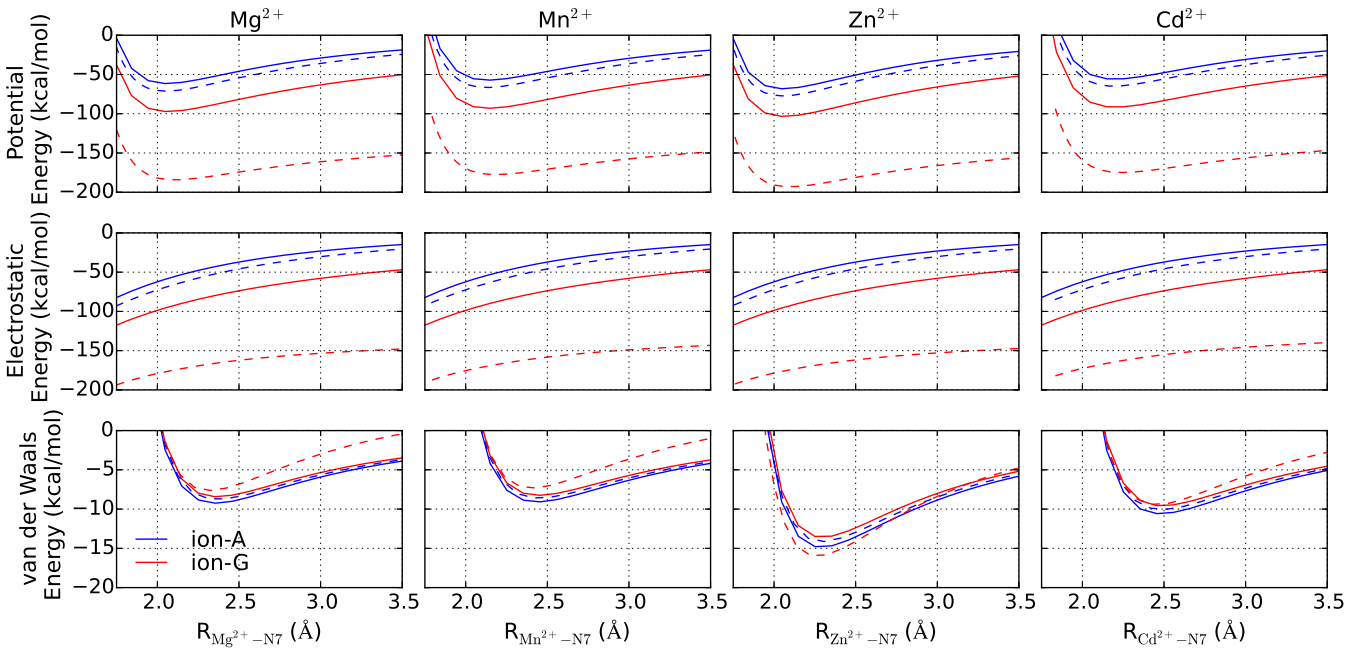

Figure S5: Summary of the rigid (solid lines) and relaxed (dashed lines) gas phase binding energy scans, along with the electrostratic and van der Waals contributions for all the metal ion - nucleoside interactions using the 12-6-4 metal ion parameters.

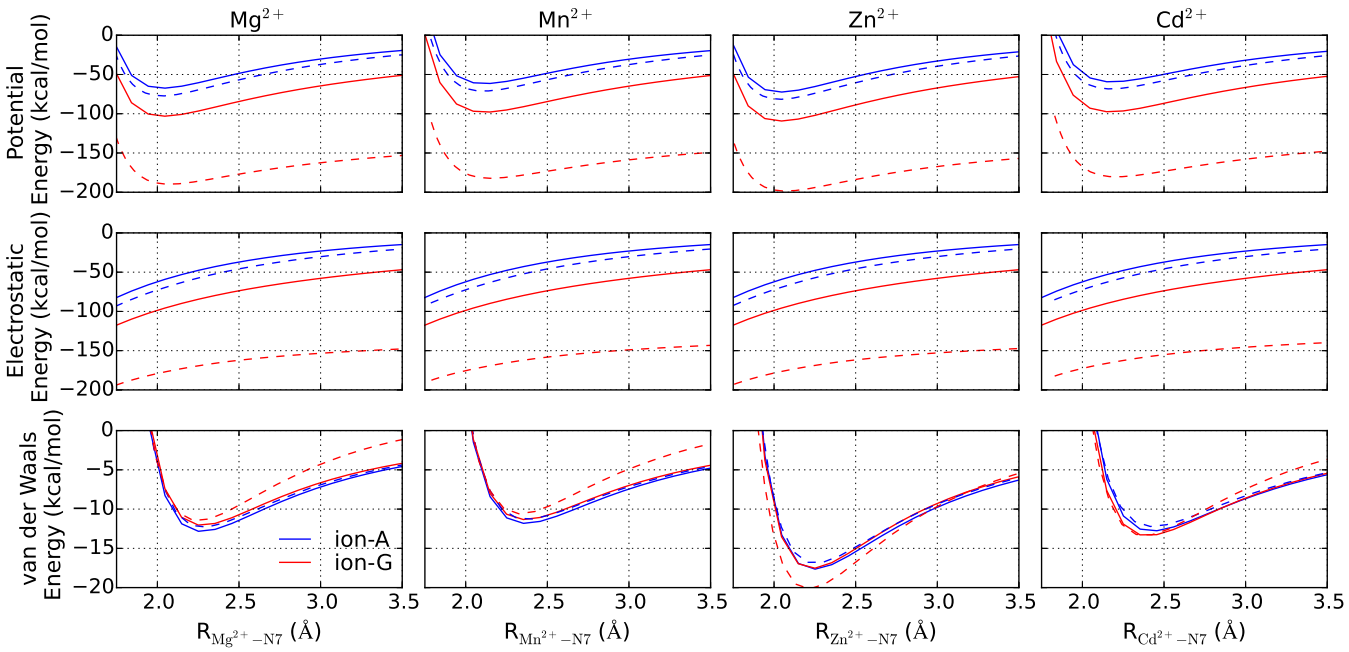

Figure S6: Summary of the rigid (solid lines) and relaxed (dashed lines) gas phase binding energy scans, along with the electrostratic and van der Waals contributions for all the metal ion - nucleoside interactions using the m12-6-4 metal ion parameters.

Applying 12-6-4 and m12-6-4 ion models to a biologically relevant system: The hammerhead ribozyme

System setup

A pre-equilibrated rhombododecahedron box of TIP4PEw[2] waters with approximately 20 Å clearance between the solute and the edge of the box was constructed. The starting structure for the simulation was initially obtained from the crystal stucture with PDB ID 2OEU,[3] resolved at 2.00 Å resolution, and was modified as follows before being immersed into the pre-equilibrated water box. At the 5′-terminal end of chain A, GTP was changed to G5′ while on chain B, the O2′-methylated C6, 5-bromo substituted U11 and deoxy C20 nucleophile were changed to C, U and C respectively. The five Mn^{2+} ions present were also converted to Mg^{2+} ions. Crystallographic

waters were retained and a NaCl[4] concentration of approximately 0.14 M was added.

MD simulations

The reactant and precursor states of the hammerhead ribozyme were simulated for 60 ns and representative snapshots from these two simulations were utilized as starting structures for the umbrella sampling simulations from which metal ion migration profiles were ultimately obtained.

Simulation protocol

The two hammerhead ribozyme MD simulations were carried out using the NAMD simulation package (version 2.9)[5] with the AMBER FF14 force field[6–9] and TIP4PEw water model.[2] Parameters for the deprotonated nucleophile were generated according to the FF14 force field and partial atomic charges were obtained using the standard RESP fitting procedure.[10] The Allner *et al.* Mg^{2+} parameters[11] were also employed. Particle Mesh Ewald summation was utilized to treat long-range electrostatic interactions[12,13] and a 9 Å cutoff was applied for non-bonded interactions. The temperature was maintained at 300K with a Langevin thermostat[14] and pressure was controlled with the Nosé-Hoover-Langevin pressure piston.[15] Both periodic boundary conditions and SHAKE[16] constraints for bonds involving hydrogens were utilized. The equations of motion were integrated with a 1 fs timestep and coordinates were outputted every 1 ps. Simulations were equilibrated in two steps: 1) 1 ns solvent/ion equilbration with position restraints of 1 kcal/mol placed on solute atoms followed by 2) 6 ns solute equilibration where exponentially decaying distance restraints, from 25.0 to 0.0 kcal/mol (heavy atom distance 2.8 Å, hydrogen distance 1.8 Å), were applied to maintain several key interactions (Table S4).

Table S4: Hammerhead equilibration distance restraints

State	Interaction	Restraint distance (Å)	Crystal distance (Å)
Reactant	A9:OP2—MG301	2.00	2.00
	G10.1:N7—MG301	2.00	2.00
	C1.1:O5′—G8:HO2′	1.80	2.50
	C1.1:OP2—G8:HO2′	1.80	2.40
	C17:O2′—G12:N1	2.80	3.25
Precursor	A9:OP2—MG301	2.00	2.00
	G10.1:N7—MG301	2.00	2.00
	C1.1:O5′—G8:HO2′	1.80	2.50
	C1.1:OP2—G8:HO2′	1.80	2.40
	C17:O2′—G12:H1	1.80	2.50
	C17:O2′—G12:H21	1.80	2.50

Metal ion migration free energy profiles

All the free energy profiles are characterized by a bimodal landscape with a local minimum at a reaction coordinate value of 0 (although for Cd^{2+} this is less pronounced), where a reaction coordinate value of 0 represents equivalent distances for both these contacts. Thus, all ion models are making direct contacts at this point in the reaction coordinate across both reactant and precursor ribozyme states. Regardless of parameter set or ribozyme state, Mg^{2+} and Zn^{2+} maintain distances of approximately 2.14 and 2.12 Å, respectively, at this local minimum while Mn^{2+} and Cd^{2+} show different coordinating behavior depending on both parameter type and reaction state. Namely, the Mn^{2+} - G10.1:N7 and C17:OP distances shift down by 0.2 Å to 2.20 Å in the reactant state when using the m12-6-4 parameters versus the 12-6-4 parameters while this coordinating distance for Mn^{2+} in the precursor ribozyme state is not really affected by parameter type (2.20 vs. 2.17 Å). For Cd^{2+}, the average coordinating distance at this local minimum is larger in the precursor state compared to the reactant state, and for a particular ribozyme state, the m12-6-4 model leads to shorter distances versus the original 12-6-4 Cd^{2+} model. The average absolute distances along the reaction coordinate between both G10.1:N7 and C17:OP and the ion are summarized in Figure S6 for all umbrella sampling simulations.

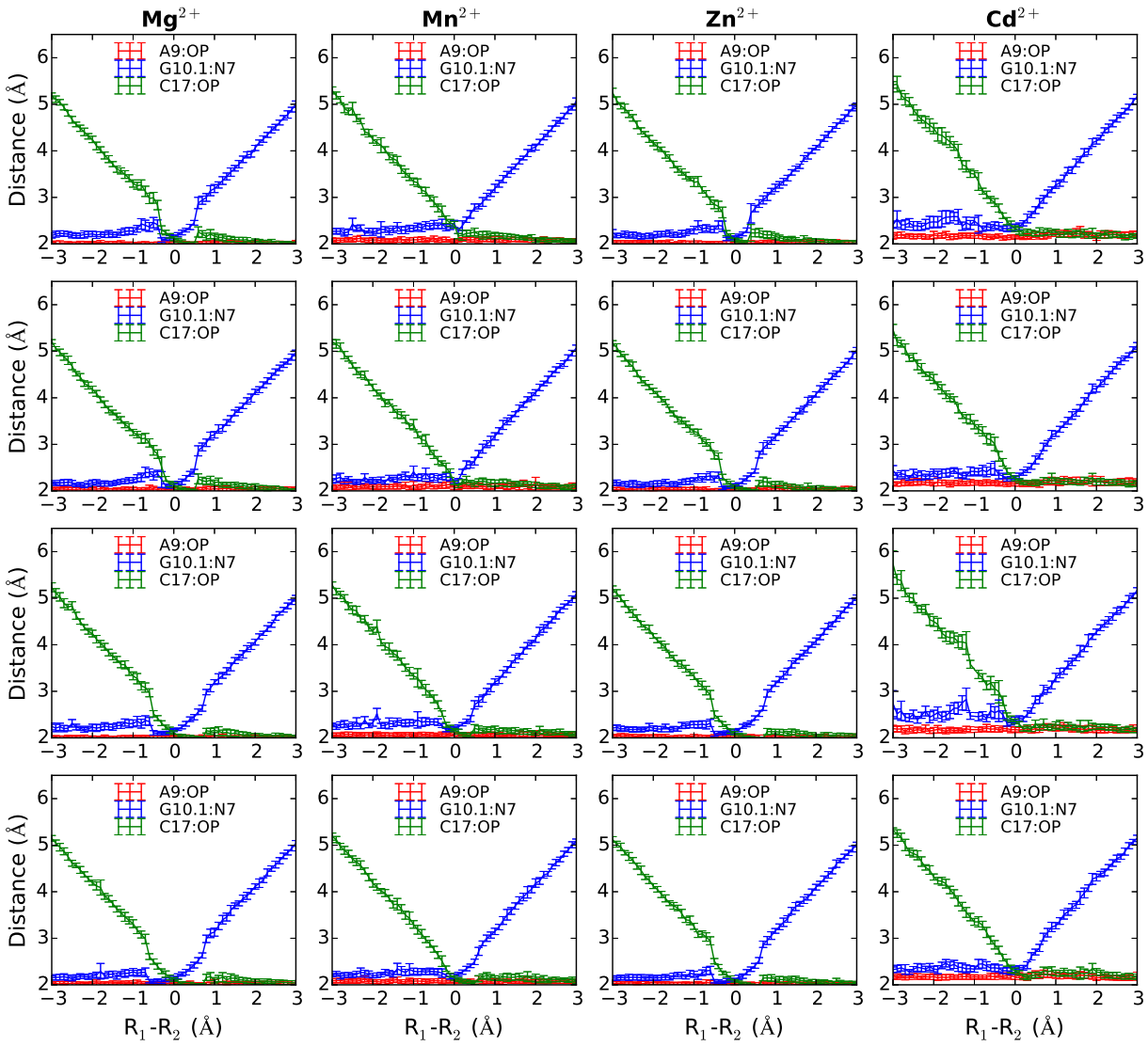

Figure S7: Free energy profiles were performed for two ns and the last 1.5 ns was used for analysis. Each subplot shows the average distances and standard deviations for the three key distances that define the binding of the ion to the two binding sites: ion - G10.1:N7 (blue), ion - A9:OP (red) and ion - C17:OP (green). We define the reaction coordinate as the difference in ion - G10.1:N7 and ion - C17:OP distances, labeled as R_1-R_2, where the ion - A9:OP contact is maintained in both binding sites. Each column repesents metal ion migration of either Mg^{2+}, Mn^{2+}, Zn^{2+} or Cd^{2+} and each row represents a specific combination of ribozyme state and ion parameters for which the metal ion migration profile was obtained. Row 1: Reactant state of ribozyme with original 12-6-4 ion parameters, Row 2: Reactant state with m12-6-4 ion models, Row 3: Precursor state of ribozyme with original 12-6-4 ion parameters, Row 4: Precursor state with m12-6-4 ion models. Details on the ribozyme states and the binding sites for the metal ion migration can be found in the main text.

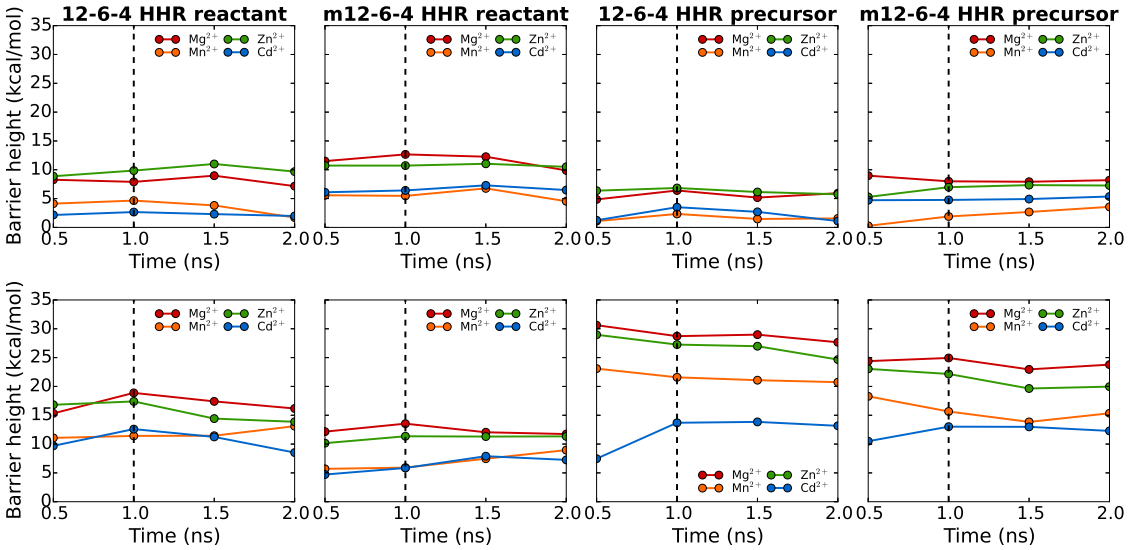

Figure S8: Barrier heights for metal ion migration of 12-6-4 and m12-6-4 Mg^{2+}, Mn^{2+}, Zn^{2+} and Cd^{2+} ion models in the hammerhead ribozyme (HHR) reactant and precursor states. Each data point on the plot represents the computed barrier height for a 0.5 ns segment up to that point. The final reported barriers and error estimates were obtained by averaging the barriers from the last 1.5 ns and taking their standard deviations. Top: Activation free energy barriers for migrating from the C-site to the bridging site and Bottom: Activation free energy barriers for ion migration from the bridging site to the C-site.

Table S5: Key features of hammerhead ribozyme (HHR) metal ion migration free energy profiles considering different ion parameters and ribozyme states. R_{min1} and R_{min2} are the reaction coordinate values for the first and second ion binding sites, respectively, where the reaction coordinate is defined as a difference in two distances (G10.1:N7-ion distance - C17:OP-ion distance). ΔG_1 and ΔG_2 are the free energy barriers associated with going from the first binding site to the second and vice versa. Standard deviations come from three consecutive 0.5 ns segments of data.

	Environment	R_{min1}	ΔG_1	R_{min2}	ΔG_2
Mg^{2+}	12-6-4, HHR reactant	-2.12 $\pm$ 0.04	8.1 $\pm$ 0.7	2.37 $\pm$ 0.07	17.5 $\pm$ 1.1
	m12-6-4, HHR reactant	-1.82 $\pm$ 0.01	11.6 $\pm$ 1.2	2.29 $\pm$ 0.06	12.4 $\pm$ 0.8
	12-6-4, HHR precursor	-2.12 $\pm$ 0.02	5.8 $\pm$ 0.5	2.87 $\pm$ 0.02	28.5 $\pm$ 0.6
	m12-6-4, HHR precursor	-2.25 $\pm$ 0.04	8.0 $\pm$ 0.1	2.85 $\pm$ 0.04	23.9 $\pm$ 0.8
Mn^{2+}	12-6-4, HHR reactant	-1.87 $\pm$ 0.11	3.4 $\pm$ 1.2	2.25 $\pm$ 0.05	12.0 $\pm$ 0.8
	m12-6-4, HHR reactant	-1.68 $\pm$ 0.04	5.6 $\pm$ 0.9	2.23 $\pm$ 0.01	7.4 $\pm$ 1.2
	12-6-4, HHR precursor	-1.72 $\pm$ 0.00	1.8 $\pm$ 0.4	2.82 $\pm$ 0.02	21.1 $\pm$ 0.3
	m12-6-4, HHR precursor	-1.94 $\pm$ 0.12	2.7 $\pm$ 0.7	2.87 $\pm$ 0.02	14.9 $\pm$ 0.8
Zn^{2+}	12-6-4, HHR reactant	-1.94 $\pm$ 0.03	10.2 $\pm$ 0.6	2.43 $\pm$ 0.04	15.2 $\pm$ 1.6
	m12-6-4, HHR reactant	-2.03 $\pm$ 0.04	10.8 $\pm$ 0.2	2.36 $\pm$ 0.07	11.3 $\pm$ 0.2
	12-6-4, HHR precursor	-1.89 $\pm$ 0.03	6.2 $\pm$ 0.5	2.87 $\pm$ 0.03	26.3 $\pm$ 1.2
	m12-6-4, HHR precursor	-1.60 $\pm$ 0.01	7.2 $\pm$ 0.2	2.90 $\pm$ 0.03	20.6 $\pm$ 1.1
Cd^{2+}	12-6-4, HHR reactant	-1.77 $\pm$ 0.05	2.3 $\pm$ 0.3	2.33 $\pm$ 0.06	10.8 $\pm$ 1.7
	m12-6-4, HHR reactant	-2.27 $\pm$ 0.08	6.7 $\pm$ 0.4	2.40 $\pm$ 0.13	7.0 $\pm$ 0.9
	12-6-4, HHR precursor	-1.84 $\pm$ 0.06	1.9 $\pm$ 1.2	2.64 $\pm$ 0.04	13.3 $\pm$ 0.2
	m12-6-4, HHR precursor	-2.03 $\pm$ 0.09	5.0 $\pm$ 0.3	2.60 $\pm$ 0.09	12.8 $\pm$ 0.3

References

(1) Sigel, R. K. O.; Sigel, H. A stability concept for metal ion coordination to single-stranded nucleic acids and affinities of individual sites. *Acc. Chem. Res.* **2010**, *43*, 974–984.

(2) Horn, H. W.; Swope, W. C.; Pitera, J. W.; Madura, J. D.; Dick, T. J.; Hura, G. L.; Head-Gordon, T. Development of an improved four-site water model for biomolecular simulations: TIP4P-Ew. *J. Chem. Phys.* **2004**, *120*, 9665–9678.

(3) Martick, M.; Lee, T.-S.; York, D. M.; Scott, W. G. Solvent structure and hammerhead ribozyme catalysis. *Chem. Biol.* **2008**, *15*, 332–342.

(4) Joung, I. S.; Cheatham III, T. E. Determination of alkali and halide monovalent ion parameters for use in explicitly solvated biomolecular simulations. *J. Phys. Chem. B* **2008**, *112*, 9020–9041.

(5) Phillips, J. C.; Braun, R.; Wang, W.; Gumbart, J.; Tajkhorshid, E.; Villa, E.; Chipot, C.; Skeel, R. D.; Kaleé, L.; Schulten, K. Scalable molecular dynamics with NAMD. *J. Comput. Chem.* **2005**, *26*, 1781–1802.

(6) Cornell, W. D.; Cieplak, P.; Bayly, C. I.; Gould, I. R.; Merz, Jr., K. M.; Ferguson, D. M.; Spellmeyer, D. C.; Fox, T.; Caldwell, J. W.; Kollman, P. A. A second generation force field for the simulation of proteins, nucleic acids and organic molecules. *J. Am. Chem. Soc.* **1995**, *117*, 5179–5197.

(7) Wang, J.; Cieplak, P.; Kollman, P. A. How well does a restrained electrostatic potential (RESP) model perform in calculating conformational energies of organic biological molecules. *J. Comput. Chem.* **2000**, *21*, 1049–1074.

(8) Pérez, A.; Marchán, I.; Svozil, D.; Sponer, J.; Cheatham III, T. E.; Laughton, C. A.; Orozco, M. Refinement of the AMBER force field for nucleic acids: Improving the description of α/γ conformers. *Biophys. J.* **2007**, *92*, 3817–3829.

(9) Zgarbová, M.; Otyepka, M.; Šponer, J.; Mládek, A.; Banáš, P.; Cheatham III, T. E.; Jurečka, P. Refinement of the Cornell et al. nucleic acids force field based on reference quantum chemical calculations of glycosidic torsion profiles. *J. Chem. Theory Comput.* **2011**, *7*, 2886–2902.

(10) Bayly, C. I.; Cieplak, P.; Cornell, W. D.; Kollman, P. A. A well-behaved electrostatic potential based method using charge restraints for deriving atomic charges: The RESP model. *J. Phys. Chem.* **1993**, *97*, 10269–10280.

(11) Allnér, O.; Nilsson, L.; Villa, A. Magnesium ion-water coordination and exchange in biomolecular simulations. *J. Chem. Theory Comput.* **2012**, *8*, 1493–1502.

(12) Darden, T.; York, D.; Pedersen, L. Particle mesh Ewald: An N log(N) method for Ewald sums in large systems. *J. Chem. Phys.* **1993**, *98*, 10089–10092.

(13) Essmann, U.; Perera, L.; Berkowitz, M. L.; Darden, T.; Hsing, L.; Pedersen, L. G. A smooth particle mesh Ewald method. *J. Chem. Phys.* **1995**, *103*, 8577–8593.

(14) Brünger, A.; Brooks III, C. L.; Karplus, M. Stochastic boundary conditions in molecular dynamics simulations of ST2 water. *Chem. Phys. Lett.* **1984**, *105*, 495–500.

(15) Feller, S.; Zhang, Y.; Pastor, R.; Brooks, B. Constant pressure molecular dynamics simulation: The Langevin piston method. *J. Chem. Phys.* **1995**, *103*, 4613–4621.

(16) Miyamoto, S.; Kollman, P. A. SETTLE: An analytic version of the SHAKE and RATTLE algorithms for rigid water models. *J. Comput. Chem.* **1992**, *13*, 952–962.